Characterizing ultrashort laser pulses with second harmonic dispersion scans

Ivan Sytcevich,[1,†,*] Chen Guo,[1,†] Sara Mikaelsson,[1] Jan Vogelsang,[1,2]
Anne-Lise Viotti,[1] Benjamín Alonso,[3] Rosa Romero,[4] Paulo T. Guerreiro,[4]
Íñigo J. Sola,[3] Anne L'Huillier,[1] Helder Crespo,[4,5,6] Miguel Miranda,[1,4]
and Cord L. Arnold[1]

[1]Department of Physics, Lund University, Box 118, 22100 Lund, Sweden
[2]NanoLund, Lund University, Box 118, 22100 Lund, Sweden
[3]Grupo de Aplicaciones del Láser y Fotónica (ALF), Departamento de Física Aplicada, University of Salamanca, Plaza de la Merced s/n 37008 Salamanca, Spain
[4]Sphere Ultrafast Photonics, Rua do Campo Alegre, 1021, Edifício FC6, 4169-007 Porto, Portugal
[5]IFIMUP-IN and Departamento de Física e Astronomia, Universidade do Porto, Rua do Campo Alegre 687, 4169007 Porto, Portugal
[6]Present address: Blackett Laboratory, Imperial College, London SW7 2AZ, UK
*Corresponding author: ivan.sytcevich@fysik.lth.se

The dispersion scan (d-scan) technique has emerged as a simple-to-implement characterization method for ultrashort laser pulses. D-scan traces are intuitive to interpret and retrieval algorithms that are both fast and robust have been developed to obtain the spectral phase and the temporal pulse profile. Here, we shortly review the second harmonic generation d-scan technique, focusing predominantly on results obtained at the Lund Laser Centre. We describe and compare recent implementations for the characterization of few- and multi-cycle pulses as well as two different approaches for recording d-scan traces in a single shot, thus showing the versatility of the technique.   © 2021 Optical Society of America

https://doi.org/10.1364/JOSAB.412535

1. INTRODUCTION

Ultrashort laser pulses have become an indispensable tool in numerous fields of science and engineering and find multiple applications in physics, chemistry, materials processing, and medicine. Almost directly after the invention of the laser, the introduction of passive mode-locking techniques led to light pulses with durations in the picosecond (ps) range [1,2]. The discovery of titanium:sapphire as a laser-active material in the mid-1980s [3], together with chirped pulse amplification (CPA) [4] and Kerr-lens mode locking [5], resulted in rapid commercialization and spread of the technology. Advanced nonlinear post-compression techniques [6–8] have led to pulses with durations down to only a few femtoseconds in the visible and near-infrared (NIR) spectral regions. In this regime, the pulse envelope contains only a few oscillations of the electric field, which gives access to a variety of exciting physical phenomena [9,10]. Such ultrashort pulses can be used to produce even shorter waveforms by the process of high-order harmonic generation [11,12], which further pushes achievable pulse widths down to the attosecond regime [13–15], allowing experimental studies with unprecedented time resolution.

Many applications of ultrashort laser pulses require their accurate characterization, i.e., the determination of the exact waveform of the laser pulse or, at the least, of its intensity profile. Both are challenging tasks, since it is not easy to directly access the pulse information in the time domain. Direct time-resolved diagnostics (e.g., attosecond streaking [16], petahertz (PHz) oscilloscope [17], tunneling ionization with a perturbation for the time-domain observation of an electric field (TIPTOE) [18], and electro-optic sampling-based approaches [19]) have been demonstrated. These techniques, however, often require powerful phase-stable laser pulses and complex setups. Less demanding experimental approaches have been proposed to characterize ultrashort pulses. The intensity autocorrelation measurement was one of the first techniques to be introduced [20] and is still widely used. It records the intensity of a non-linear signal (usually the second harmonic) as a function of the delay between two pulse replicas to obtain an estimate of the duration of the pulse temporal profile. The exact pulse amplitude and the phase information remain, however, unavailable [21]. By adding a spectrometer to the detection scheme and measuring a spectrum at each delay, a two-dimensional (2D) spectrogram can be obtained, which is the basis of the

frequency-resolved optical gating (FROG) [22–24] technique. With the use of iterative mathematical algorithms, both phase and amplitude can be retrieved and the pulse reconstructed. Another popular approach, named spectral phase interferometry for direct electric-field reconstruction (SPIDER) [25–27], relies on recording a spectral interference pattern between two delayed and frequency-sheared pulse replicas. Compared to FROG, this method does not require complex retrieval algorithms at the expense of a more complicated optical setup.

A different class of characterization techniques does not rely on pulse replicas, but manipulates the pulse in the spectral domain. In multiphoton intrapulse interference phase scan (MIIPS), a spectral phase shaper is typically used to apply controlled phase functions to the pulse while the second harmonic spectrum is measured [28]. The group delay dispersion (GDD) curve can be obtained by establishing which function locally cancels out the original spectral phase and therefore maximizes the second harmonic generation (SHG) output at each wavelength, thus allowing the retrieval of the spectral phase and consequently the reconstruction of the temporal pulse profile. Besides MIIPS, related approaches also utilizing pulse shapers have been reported, namely DazScope and later Chirpscan [29,30]. These are most commonly implemented with programmable dispersive filters, which are very common in CPA chains.

The dispersion scan (d-scan) utilizes a similar concept [31,32]. A spectral phase is applied to the pulse to be characterized, typically by simply introducing a glass wedge pair. By changing the amount of dispersion, e.g., by moving glass wedges of variable thickness in the beam and recording the spectrum of a nonlinear signal (second harmonic, for instance), a 2D trace is produced. The innovative feature of the d-scan technique is the phase retrieval approach: in a similar fashion to FROG, it uses all of the trace information to recover the spectral phase using iterative algorithms. This approach comes at an extra cost of algorithm complexity and computational power, but brings important advantages, namely in terms of bandwidth and feedback on the quality of the measurement. All of the techniques mentioned above create 2D traces that are formally equivalent, and it is possible to use them interchangeably (e.g., use a MIIPS analysis on a trace made simply with glass wedges or an iterative phase retrieval using a ChirpScan or d-scan algorithm on a MIIPS trace) [33]. There are, however, trade-offs that make one technique more convenient than the other, depending on each specific case.

One of the main advantages of the d-scan is the simple in-line setup without the need for pulse replicas or spectral shearing. Furthermore, d-scan often uses a compressor—an essential building block of almost any ultrafast laser—to manipulate the spectral phase, and thus allows for simultaneous compression and characterization of ultrashort light pulses. Since its invention, the d-scan has become a well-established technique in many laboratories around the world. It has been implemented and tested with different target pulse widths and central frequencies, and d-scan-compressed pulses have enabled a variety of applications ranging from pump-probe spectroscopy to biomedical imaging [34–37].

In this paper, we discuss the main features of the d-scan technique, mostly focusing on SHG as a nonlinear process, and present recent developments and results predominantly

obtained at the Lund Laser Centre (LLC). In section 2, we provide a basic theoretical description and introduce the mathematical framework needed to describe a d-scan measurement. We give insights on how to interpret d-scan traces and how to choose phase retrieval strategies. In section 3, we describe different experimental implementations of the technique, for a wide range of pulse durations and wavelengths. Next, we present single-shot methods and discuss the advantages and limitations of using d-scan as a single-shot technique (section 4). Finally, we conclude and give an outlook towards future developments of the method.

2. THEORY

A. Concept of a D-Scan Measurement

We first provide a simple theoretical description and discuss generic properties of d-scan measurements. This will further help with the understanding of the advantages and limitations of this characterization technique as well as the reasoning behind certain engineering solutions.

The complex electric field representing a laser pulse can be expressed in the frequency domain as

$$\tilde{U}(\omega) = |\tilde{U}(\omega)| \exp[i\phi(\omega)] = \int_{-\infty}^{\infty} U(t) \exp(-i\omega t)\mathrm{d}t, \quad \textbf{(1)}$$

where $|\tilde{U}(\omega)|$ is the spectral amplitude, $\phi(\omega)$ is the spectral phase, and $U(t)$ is the corresponding complex electric field in the time domain. Propagating the pulse through a transparent medium of thickness z is equivalent to multiplying Eq. (1) with a phase term:

$$\tilde{U}(z, \omega) = |\tilde{U}(\omega)| \exp[i\phi(\omega)] \cdot \exp[ik_0(\omega)n(\omega)z], \quad \textbf{(2)}$$

where n is the refractive index of the medium, and k_0 is the vacuum wavenumber.

Pulse measurement techniques usually employ a nonlinear process in order to obtain pulse amplitude and phase sensitivity. Mathematically, the result of a nonlinear interaction can be written as

$$U_{\mathrm{NL}}(z, t) = f\left[\int_{-\infty}^{\infty} \tilde{U}(z, \omega) \exp(i\omega t)\mathrm{d}\omega\right], \quad \textbf{(3)}$$

where f represents the particular nonlinear interaction. In this article, we mainly deal with SHG d-scan, where f simply stands for squaring. Finally, the power spectrum of the process is measured as a function of dispersion, and a 2D trace is obtained:

$$I(z, \omega) = \left|\int_{-\infty}^{\infty} U_{\mathrm{NL}}(z, t) \exp(-i\omega t)\mathrm{d}t\right|^2. \quad \textbf{(4)}$$

The simple model presented above assumes an ideal coupling of the fundamental radiation to the nonlinear signal, which implies perfect phase matching over the pulse bandwidth. For broadband few-cycle pulses, it is usually not the case [38,39], and a response function $R(\omega)$ (which may contain not only the effect of finite phase matching, but also technical parameters, e.g., a spectrometer response function) has to be included to accommodate for the irregular spectral response,

$$I_{\mathrm{real}}(z, \omega) = R(\omega) \cdot I_{\mathrm{ideal}}(z, \omega). \quad \textbf{(5)}$$
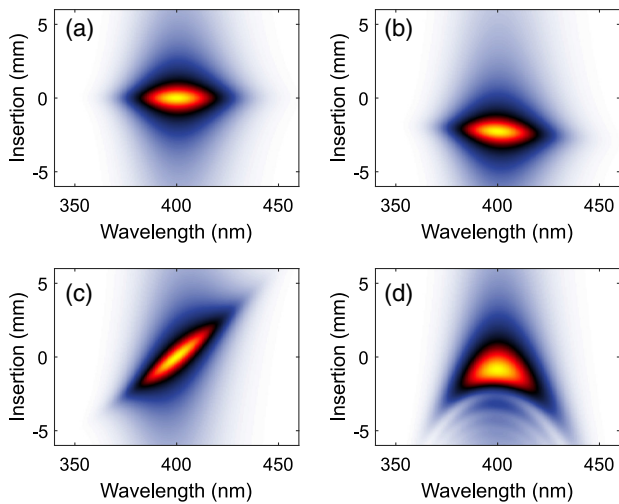
Fig. 1. Simulated SHG d-scan traces for a 10 fs Gaussian pulse centered at 800 nm with (a) no phase applied, (b) 100 fs^2 GDD, (c) 800 fs^3 TOD, and (d) 8000 fs^4 FOD.

A second harmonic d-scan trace for an ideal 10 fs full width at half-maximum (FWHM) Gaussian pulse with a center wavelength of 800 nm is presented in Fig. 1(a). In this simulation, the index of refraction is calculated from the Sellmeier equation for BK7 glass, which is a common material used for d-scan wedges in the visible and NIR spectral ranges. In Figs. 1(b)–1(d), we add numerically different dispersion orders in the Taylor expansion of the spectral phase, i.e., GDD, third-order dispersion (TOD), and fourth-order dispersion (FOD). Applying a positive GDD to the pulse mainly shifts the trace down along the dispersion axis [Fig. 1(b)], implying that the pulse can be re-compressed by removing glass. The trace appears to be slightly tilted, due to the fact that BK7 introduces not only GDD, but also higher-order terms. This becomes more obvious in Fig. 1(c), where a d-scan trace with TOD is shown, resulting in an almost linear tilt of the trace with respect to the dispersion axis. Finally, FOD leads to a parabolic-like deformation [Fig. 1(d)]. These simple examples highlight the sensitivity of d-scan measurements to the spectral phase of the pulse. The d-scan trace therefore provides an intuitive way to visually assess the quality of compressed pulses, even without using reconstruction algorithms, which is a very useful day-to-day optimization metric for, e.g., few-cycle pulses from hollow-core fiber (HCF) compressors [40,41]. Following from the examples illustrated in Fig. 1, it should be noted that neither the absolute spectral phase nor its slope (corresponding to a delay in the time domain) are essential for the temporal intensity profile or the obtained d-scan trace, but only its second- and higher-order derivatives.

B. Phase Retrieval

It is a straightforward procedure to calculate a d-scan trace for a known pulse. However, the reverse, i.e., extracting information *from* a measured d-scan trace, is not such a trivial task. Mathematically, this falls into the class of inverse problems and is tackled by mathematical routines named phase retrieval algorithms. The main idea is to find the pulse that generates a nearly identical trace compared to the experimental data. Numerically, we seek to minimize a root mean square (RMS)

error G between the experimentally measured and the computed trace, sampled with $m = 1, 2, \cdots N_m$ points in frequency and $k = 1, 2, \cdots N_k$ different glass insertions:

$$G^2 = \frac{1}{N_m N_k} \sum_{m,k} (I_{\mathrm{meas}}(\omega_m, z_k) - \mu_m I_{\mathrm{retr}}(\omega_m, z_k))^2. \quad \textbf{(6)}$$

Here, I_{meas} and I_{retr} are the measured and simulated traces, respectively, and

$$\mu_m = \sum_k \left[I_{\mathrm{meas}}(\omega_m, z_k) I_{\mathrm{retr}}(\omega_m, z_k) \right] / \sum_k I_{\mathrm{retr}}(\omega_m, z_k)^2 \quad \textbf{(7)}$$

is a minimization factor that is calculated and updated in every iteration. For a successful retrieval, μ_m gives the spectral response function $R(\omega)$ [Eq. (5)].

Equation (6) shows that pulse retrieval by minimizing G essentially is a nonlinear least-squares problem. Solving such problems is a well-studied field of mathematics. Least-squares minimization routines like Nelder–Mead (NM), Levenberg–Marquardt (LM), or Broyden–Fletcher–Goldfarb–Shanno algorithms can be readily implemented as pulse retrievers and are used extensively with d-scan. The NM or downhill simplex, a method that was predominantly used in early d-scan works [31,32], proved to be robust and reliable, albeit slow. The usage of LM-based minimization was reported in a self-calibrating d-scan technique, where the compressor parameters, i.e., introduced dispersion, could also be retrieved from the measurement [42]. This, in turn, allowed the quantification and elimination of pulse train instabilities in supercontinuum fiber lasers [43]. Another example is the d-scan retrieval algorithm based on differential evolution [44], which, besides a faster convergence compared to NM, was shown to be less prone to stagnate in local minima. In general, in order to use this type of algorithm efficiently, it is beneficial to choose a convenient parametrization of the spectral phase. Expansion into a Fourier series usually increases the convergence speed, but, in certain cases, also the risk to get stuck in local minima. A possible workaround to this issue is to use a spline interpolation instead [45] or to switch to a different parametrization whenever stagnation happens [31]. For long, "clean" pulses, which often have simple d-scan traces, a Taylor series representation of the phase can also be used. Phase parametrizations and retrieval strategies may also build on manipulating only second- and higher-order derivatives of the spectral phase.

Another class of retrieval algorithms, often used with FROG, is that of iterative constraint-based inversion algorithms (e.g., generalized projections or ptychography-based approaches), inspired by early work in diffractive imaging [46]. The main feature of such methods is to introduce a set of certain constraints on the retrieved pulse in such a way that the error G [Eq. (6)] is reduced in each iteration. This, arguably more elegant way of solving phase retrieval problems, is often faster compared to the "brute-force" minimization mentioned previously [47,48]. However, the speed-up often comes with the price of reduced robustness, especially when dealing with traces contaminated by noise. This was recently attributed to the fact that these algorithms do not converge to the least-squares solution in the presence of Gaussian noise [49,50]. Thus, it might be preferable to choose general least-squares solvers, which were shown to be more reliable in these conditions [33]. To give an

example, an algorithm based on data (or intensity) constraint was recently proposed for d-scan phase retrieval [51]. There, the data constraint means that the amplitude for the simulated complex d-scan trace is replaced with the measured data, while the phase information is kept at each iteration of the algorithm. This method exhibits a faster convergence speed compared to the NM approach, but at the same time is significantly more susceptible to noise [51].

Generally speaking, the task of designing fast, robust, and efficient retrieval algorithms is an active field of research, and a significant amount of effort is devoted to the development of routines that are optimized for pulse characterization problems. The recently proposed common pulse retrieval algorithm (COPRA) [49,50], for example, is a general algorithm that not only works with d-scan, but with several other methods as well, like FROG or MIIPS. While being inspired by constraint-based methods, COPRA elegantly avoids the aforementioned problem of not reaching the least-squares solution by replacing a data constraint step with a gradient descent in the final stages of the algorithm run. This, in turn, helps to increase the accuracy of the retrievals for traces with high levels of Gaussian noise. Another exciting development is the use of artificial neural networks for pulse reconstruction [52], which was recently reported for d-scan as well [53], showing impressive millisecond (ms)-scale retrieval times and thus opening possibilities for "Live View" pulse monitoring when combined with a single-shot d-scan system.

3. IMPLEMENTATION

After the first demonstration of the d-scan technique in 2012 [31], which at that time focused on the characterization of pulses from few-cycle light sources in the NIR, there has been great effort to extend the applicability to pulses of different durations and central frequencies, combining various nonlinear phenomena with different approaches to introduce the required dispersion variation.

The most popular choice for nonlinear interaction in d-scan measurements is SHG, owing to the availability of nonlinear media and high signal-to-noise ratio (SNR), e.g., when compared to third-order processes. However, the use of SHG can limit the applicability of d-scan in some situations. The limited phase matching bandwidth of common SHG crystals usually reduces the effective spectral range of a single d-scan setup. The use of dielectric nanoparticles, which are free from phase matching limitations, as a nonlinear medium was recently reported [54] as one possible solution. Another issue occurs when measuring pulses with octave-spanning spectra, where there is an overlap between certain frequency components of the fundamental and second harmonic fields. In this case, the useful signal has to be carefully filtered, e.g., by using spatial masks or polarizers [55]. It is, however, worth mentioning that this usually undesirable feature can be beneficial: the produced interference of the fundamental and the SHG field is sensitive to the carrier-to-envelope phase and including this information in the retrieval algorithm allows for complete reconstruction of the electric field waveform [56].

Higher-order nonlinear processes, e.g., third harmonic generation (THG), can be utilized to alleviate these problems. D-scan setups based on THG in graphene [57] and thin films of $TiO_2 - SiO_2$ compounds [58] have been reported. These materials have large nonlinear coefficients so that the problem of lower efficiency of third-order interactions is reduced. For pulses with spectral content extending towards the ultraviolet (UV), approaches based on frequency up-conversion quickly become impractical because of the need for specialized deep UV spectrometers. Another issue is the lack of suitable nonlinear crystals for efficient frequency conversion in the UV, as strong dispersion in this region prevents broad phase matching and as, in most materials, absorption becomes significant. To tackle this issue, schemes based on degenerate nonlinear processes have been introduced, where the frequency of the nonlinear signal is the same as the driving field. One of these schemes is cross-polarized wave generation (XPW), which was successfully applied to the d-scan for characterizing pulses in the NIR [59] and the deep UV [60]. When using XPW, it is crucial to have a high degree of linear polarization in the driving field and a polarization scheme with a large extinction ratio after XPW for detecting the signal with good SNR. Another degenerate process that was used in d-scan measurements is self-diffraction [61], which enabled the simultaneous measurement of two unknown near-UV pulses [61].

Even for the case of one selected nonlinear interaction, the experimental realization of a d-scan can still differ substantially depending on the central frequency and pulse duration (spectral bandwidth), as illustrated in Fig. 2 for SHG. Generally, the longer the transform-limited pulse duration of the light source (the smaller the spectral bandwidth), the larger the d-scan window should be in order to capture the evolution of second harmonic around the point of optimal compression. For very short pulses, even small amounts of applied GDD result in significant compression/broadening, while for long pulses reaching ps widths or for pulses with large time-bandwidth product, the required GDD windows can be up to hundreds of thousands of fs^2. How much dispersion, in terms of the GDD
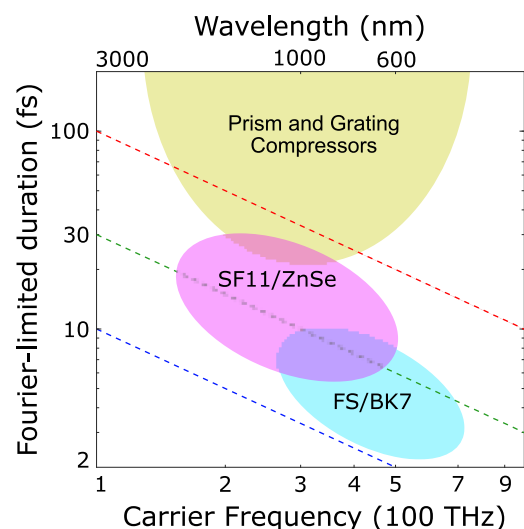
Fig. 2. SHG d-scan implementations as a function of target pulse duration and central frequency. Blue, green, and red dashed lines correspond to the duration of 1, 3, and 10 optical cycles at a given frequency, respectively. Shaded regions represent different optical components that can serve as a scanning dispersive element in a d-scan measurement. The light blue and pink areas correspond to a glass wedge pair configuration using the indicated materials.
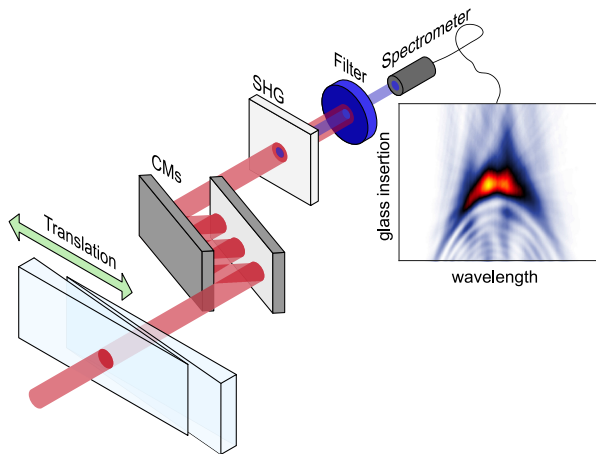
Fig. 3. SHG-based d-scan setup for the characterization of few-cycle pulses. The light passes through a compressor comprised of chirped mirrors (CMs) and glass wedge pairs; the introduced GDD is finely tuned by the movement of one of the wedges. The second harmonic signal generated in the thin crystal is detected with a spectrometer, and the trace is obtained by recording spectra at different wedge positions.

window, exactly should be scanned in order to obtain robust measurements and retrievals is not a trivial question and requires a rigorous mathematical study, which is outside of the scope of this paper. Here, we present well-contained, highly redundant, d-scan traces and instead aim at giving practical directions based on our experience when measuring pulses from different laser systems.

The early designs, using wedges made of fused silica or BK7 glass with GDD in the range of $30-50 \, \text{fs}^2/\text{mm}$, are well-suited for measuring few-cycle pulses with central frequencies in the visible and NIR, as emitted by HCF compressors or optical parametric CPA (OPCPA)-based sources [31,63,64] (light blue shaded area in Fig. 2). The use of a gas (air) dispersion for the characterization of the pulses in the deep UV has also been reported [60]. A typical second harmonic d-scan setup is presented in Fig. 3. Negative chirp is introduced by a chirped mirror pair. By finely tuning the insertion of the glass wedges and thus introducing positive GDD, the chirp can be controlled, and contributions from optical components further down the beam path towards the experiment are compensated for. A thin SHG crystal, a filter (to reject fundamental radiation), and a spectrometer are the only additional components needed to perform the measurement, making this configuration straightforward to implement. Additionally, since there is no beam splitting and recombining at any point, the required pulse energy to record a trace with a good SNR is very low, allowing measurements of pulses directly from an oscillator. In the case of amplified pulses, the measurement can be done parasitically by using only a small portion of the energy of the main pulse (e.g., reflection off a glass plate/wedge). In this work, we usually sampled the beams with minimum deviation by using the Fresnel reflection from a glass wedge in s polarization.

A d-scan trace recorded from the output of a few-cycle high-repetition rate, Ti:sapphire seeded OPCPA [65] located at LLC is shown in Fig. 4(a). A pair of BK7 glass wedges [about $45 \, \text{fs}^2/\text{mm}$ of group velocity dispersion (GVD) at 800 nm] is
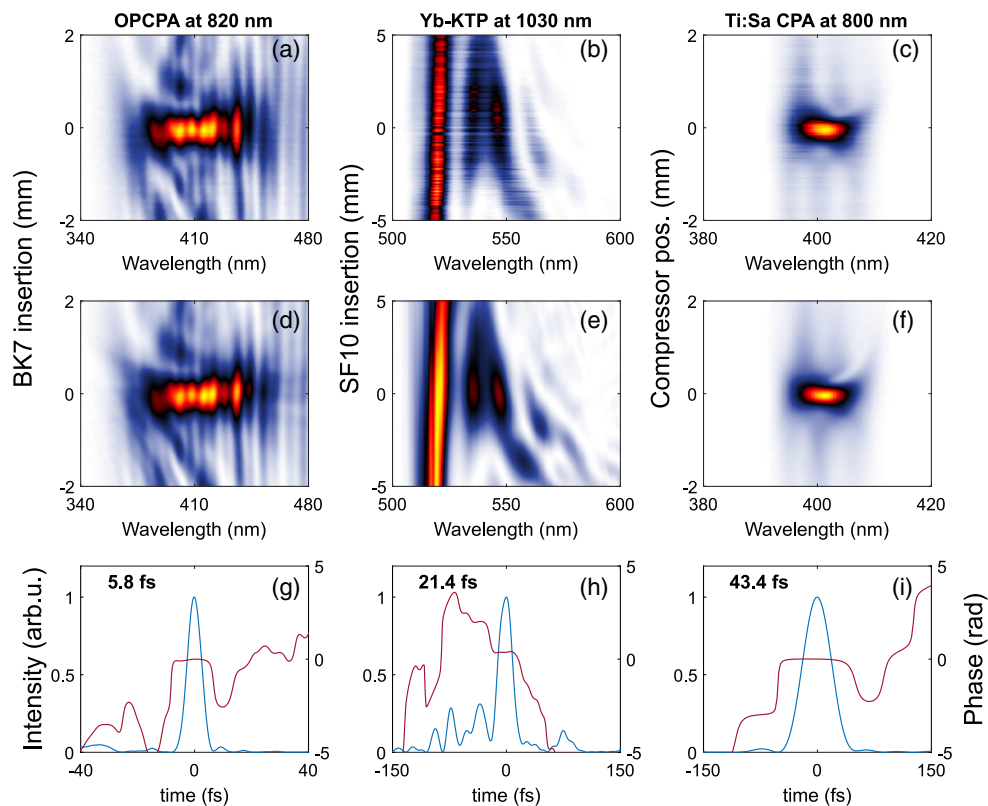

Fig. 4. SHG d-scans in different pulse duration regimes: (a)–(c) measured traces using pulses from a few-cycle OPCPA system from an Yb laser after post-compression in a KTP crystal [62] and from a 10 Hz CPA laser system, respectively; (d)–(f) corresponding retrieved traces; (g)–(i) retrieved pulse intensity profiles and phases.

used as a dispersive element, and a dispersion window of only 180 fs^2 is sufficient for the scan. The second harmonic is generated in a thin (5 μm) beta barium borate (BBO) crystal. The fundamental radiation is filtered with a polarizer, and the signal is recorded with a fiber-coupled spectrometer. Extracting the pulse information from the retrieved trace [Fig. 4(d)] gives a FWHM duration of 5.8 fs [Fig. 4(g)].

When dealing with pulses having a central wavelength further into the infrared, it is often challenging and impractical to introduce sufficient dispersion variation using wedges made from common optical glasses. With denser materials, e.g., SF10-SF57 flints, ZnS, ZnSe, etc., that have larger overall dispersion and their zero-dispersion crossings further to the infrared (compared to standard glasses), the operating range of a standard d-scan setup can be extended to longer pulses (ca. 20 fs) and wavelength regimes (<1.5 μm, indicated in pink in Fig. 2).

Figure 4(b) shows a measured d-scan trace for pulses from a solid-state ytterbium laser (1030 nm central wavelength) with a nonlinear post-compression stage in a single-domain potassium titanyl phosphate (KTiOPO$_4$ or KTP) crystal [62]. In this measurement, the d-scan setup is almost identical to the one shown in Fig. 3 with the only difference being the use of SF10 glass wedges, introducing approximately 92 fs^2/mm of GVD at 1100 nm (central wavelength of the compressed pulses, dispersion window of 920 fs^2), compared to only 19 fs^2/mm for BK7 at that wavelength. The retrieved trace [Fig. 4(e)] indicates 21.4-fs-long pulses with a series of pre-pulses in the intensity profile, originating from uncompensated TOD.

For even longer, many-cycle pulses (>25 fs), the use of prism or grating compressors can introduce appropriate amounts of dispersion (yellow region in Fig. 2). Compressors that are integral parts of amplified, short pulse lasers can be conveniently used to perform d-scans [30,42,66]. In Fig. 4(c), a d-scan measurement using a grating compressor as a dispersive element is presented. The results were obtained with a Ti:sapphire terawatt (TW)-class CPA system operated at 10 Hz, driving a high intensity attosecond pulse beamline at LLC. One of the gratings in the compressor is mounted on a motorized translation stage that was continuously moved across the point of optimal compression. The dispersion of the compressor was evaluated to be 4300 fs^2/mm of GVD. The total scanned dispersion window was 17, 200 fs^2, and the retrieval yields a pulse duration of 43.4 fs.

4. SINGLE-SHOT D-SCAN

We have so far discussed scanning d-scan implementations where the dispersion variation was applied by mechanically moving an optical element inside the pulse compressor. For laser systems with high repetition rate (>1 kHz) and good pulse-to-pulse stability, this does not affect the accuracy of the pulse characterization. The obtained d-scan trace allows for retrieval of an average pulse in the pulse train. However, for laser setups with low repetition rates or exhibiting shot-to-shot pulse duration fluctuations [which is rather common for TW-to-petawatt (PW)-level ultra-high-intensity systems], the solutions mentioned in the previous section can be either impractical, take a long time to complete, or are simply inaccurate in case of pulse
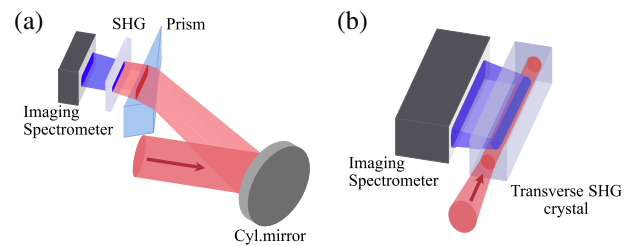

Fig. 5. Single shot d-scan schemes for measuring (a) few- and (b) multi-cycle pulses.

instabilities. Single-shot characterization techniques are more appropriate in these cases.

Single-shot FROG implementations emerged shortly after their introduction [67], while the architecture of SPIDER is fully compatible with single-shot pulse measurements [25]. The first, to the best of our knowledge, single-shot d-scan was demonstrated in 2015 [68]. In the following, the progress in the development of single-shot, SHG-based d-scan setups is shortly presented, and their performance in comparison to scanning d-scan approaches for few- and multi-cycle light pulses is discussed.

In order to perform a single-shot measurement, all moving components should be eliminated from the optical setup. Two different approaches, presented in Fig. 5, have been demonstrated so far: first, an optical element that encodes different amounts of GDD to different parts of the spatial beam profile was implemented. Second, a special nonlinear material that simultaneously introduces dispersion and nonlinearity was utilized. Common to both approaches is that the dispersion axis is translated into a spatial direction. The first approach is most conveniently implemented by replacing the scanning wedges in a standard d-scan with a prism that introduces spatially varying dispersion over the beam profile. After passing the prism, the light may be focused to a line in an SHG crystal, where different positions along the line now encode the SHG signal corresponding to different amounts of dispersion. A d-scan trace is obtained, in a single shot, if the SHG signal along the line is imaged with an imaging spectrometer.

The first, to the best of our knowledge, reported setup of that kind was designed to characterize few-cycle pulses from a HCF compressor [68]. In this experiment, a slit was used to make a line that passed a BK7 prism. The output plane of the prism was imaged onto a thin BBO crystal. Imaging is necessary to mitigate the effect of angular dispersion, which inevitably occurs at the backside of the prism. While this implementation is conceptually straightforward, the use of a slit for beam shaping can limit the SNR of the obtained d-scan traces, and the setup is quite bulky. The SNR can be improved by simply removing the slit and using the full beam profile, but a different focusing geometry is required. An elegant solution is to let the beam pass the prism first and then reflect off a spherical mirror under a large off-axis angle, introducing strong astigmatism. Adjusting the angles and distances between the prism, the mirror, and the SHG crystal allows us to focus the beam in one dimension while imaging the face of the prism in the other onto the crystal, which results in a more compact and space-efficient design [69]. A similar, but even simpler configuration, is depicted in Fig. 5(a), where the beam is focused with a cylindrical mirror to a line

onto the SHG crystal, while the prism is placed in between. The incidence angle on the mirror and the rotation of the prism have to be carefully aligned in order to minimize aberrations. Here, the angular chirp from the prism is not eliminated by imaging its output facet, but its impact is minimized by putting the SHG crystal directly after and as close to the prism as possible. As the beam is getting focused while propagating through the prism, care should be taken to avoid nonlinear effects in the prism. Finally, what is in common for all of the discussed implementations is the need for a sufficiently homogeneous beam profile—significant intensity variations across the beam can decrease the accuracy of the measurement. In practice, a magnifying telescope and an iris can be used prior to the setup to select the central part of the beam profile for the measurement. It should be noted that very recently, an alternative single-shot d-scan implementation was suggested, based on measuring SHG spectra from a discrete number of pulse copies that have propagated through glass plates of different thicknesses [70].

For the characterization of longer pulses, the methods discussed above become less straightforward, as the amount of dispersion variation (e.g., the glass insertion window) that can be achieved for a reasonably large beam size in a single prism is limited. An elegant alternative, that is also well-suited for longer pulses, is depicted in Fig. 5(b). In this implementation, a highly dispersive disordered nonlinear crystal (strontium barium nitrate, SBN) allowing for broadband transverse SHG (TSHG) is utilized both as the dispersive and nonlinear elements [71]. One advantage of the randomly ordered nonlinear crystal is its large dispersion in the NIR with around 500 fs^2/mm at 800 nm. An initially negatively chirped pulse (overcompensated by, e.g., chirped mirrors) gradually compresses after entering the material, and the second harmonic is generated perpendicularly to the direction of propagation. By recording the SHG with an imaging spectrometer, a d-scan trace is obtained in a single shot. For a typical crystal length of 10 mm, a total dispersion window of 5000 fs^2 is obtained, allowing for measurements of many-cycle pulses with durations up to 60 fs in the NIR spectral range [71].

To demonstrate the performance of single-shot d-scan implementations, we characterize near-single-cycle pulses after a HCF-based post-compression stage and multi-cycle pulses from standard millijoule (mJ)-level Ti:sapphire CPA systems, using the geometries shown in Figs. 5(a) and 5(b), respectively. In both cases, the SHG signals were detected with home-made imaging spectrometers, using a compact, crossed Czerny–Turner design [72], relying on divergent illumination of the grating in order to correct for astigmatism of the imaging path [73,74]. More information on the spectrometer design, e.g., distances and angles between components, can be found in [69]. A cylindrical lens before the CCD sensor [75] was added for additional aberration correction.

Figure 6 shows the results for the characterization of the few-cycle pulses. The data was taken with a laser system located at the University of Porto. The d-scan traces obtained with the scanning [Fig. 6(a)] and single-shot [Fig. 6(b)] implementations are conceptually similar, and the retrieved FWHM pulse durations equal to 3.4 fs and 3.7 fs, respectively, are in a good agreement. Both experiments show a slight tilt in the traces, indicating small amounts of uncompensated TOD, as also suggested by the pre-pulses in the retrieved intensity profiles [Fig. 6(c)]. In the frequency domain, the spectral phases agree quite well up to the wavelength $\lambda_s = 766$ nm, after which we observe an almost constant relative shift of 5.5 rad, which can be attributed to the low spectral amplitude at λ_s, locally introducing a high degree of uncertainty in the value of the phase. The calculated RMS error G was found to be equal to 0.015 and 0.07 (trace dimensions $M \times N$: 300×500 points in insertion and wavelength, respectively) for the scanning and single-shot measurements, respectively. The relatively high error for the single-shot case can be attributed to the lower SNR and imperfections of the imaging spectrometer. These lead to difficulties in retrieving the spectral phase in the low-intensity areas of the trace, which subsequently affect the agreement of certain low-intensity temporal structures outside of the main peak. In this respect, it should be noted that the RMS error G intrinsically reflects both the noise level of the experimental trace and the retrieval uncertainty [50].
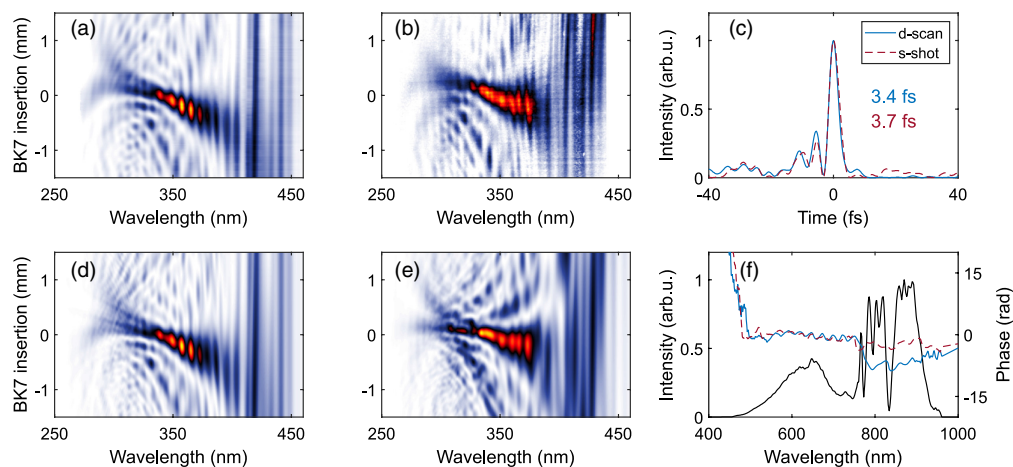

Fig. 6.   Measured traces using (a) standard and (b) single-shot (d-shot) setups for a HCF compressor system with retrievals shown in (d) and (e), respectively. (c) Retrieved pulse intensity profiles with FWHM durations indicated for both methods. (f) Measured spectrum and retrieved spectral phases. The blue lines are obtained with the scanning d-scan, while the red lines correspond to the single-shot measurements (s-shot).
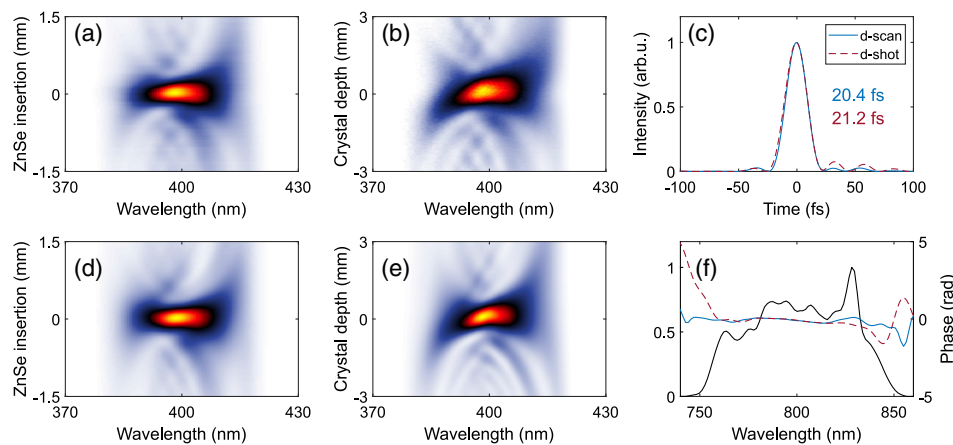
Fig. 7. Measured traces using (a) standard and (b) single-shot setups for a Ti:sapphire CPA system with retrievals shown in (d) and (e), respectively. (c) Retrieved pulse intensity profiles with FWHM durations indicated for both methods. (f) Measured spectrum and retrieved spectral phases. The blue lines are obtained with the scanning d-scan, while the red lines correspond to the single-shot measurements (d-shot).

The results from the implementation based on the random nonlinear crystal [Fig. 5(b)] are summarized in Fig. 7. The measurements were performed with a 1 kHz, mJ-level, Ti:sapphire CPA laser system at LLC, emitting near transform-limited pulses with duration around 20 fs (FHWM). The conventional (scanning) d-scan measurement, shown in Fig. 7(a), utilized a pair of ZnSe wedges, featuring extremely large dispersion (GVD = 1025 fs^2/mm) in the NIR. An acousto-optic programmable dispersive filter (Dazzler, Fastlite), which is an integral part of the CPA chain, was used to introduce negative chirp. The single-shot setup used a 10-mm-long SBN crystal with GVD of 480 fs^2/mm at 800 nm. The results are shown in Fig. 7(b). Again, the experimental traces are in good agreement, while the difference in width can be attributed to slightly different range of dispersion windows and a larger amount of residual TOD for the single-shot measurement. The pulse retrievals agree very well between the two setups in terms of the temporal intensity profiles [Fig. 7(c)] and retrieved spectral phases [Fig. 7(d)]. The RMS errors are 0.004 for the scanning d-scan ($M \times N = 300 \times 500$) and 0.019 for the single-shot version ($M \times N = 422 \times 500$), respectively.

5. CONCLUSION

In this work, we briefly reviewed the progress of pulse characterization using the second harmonic dispersion scan technique. We show that the traces obtained with d-scan are naturally very intuitive to interpret, with different polynomial contributions to the pulse spectral phase appearing as characteristic deformations of the trace. We also give a brief overview of common phase reconstruction algorithms, which can be implemented to retrieve the exact pulse information. By employing different pulse compressor configurations, the d-scan can be successfully adapted to the measurement of pulses with different pulse durations and central frequencies. Furthermore, we discuss two different single-shot implementations, well-suited for the characterization of pulse sources with low repetition rate or substantial pulse-to-pulse fluctuations, where the conventional

(scanning) d-scan would either take an inconveniently long time or result in misleading conclusions.

While the d-scan so far has been primarily used for the characterization of pulses in the NIR spectral range, derived from Ti:sapphire or ytterbium-doped lasers, the adaptation to other wavelength ranges is straightforward. In recent years, there has been a great deal of progress in the development of light sources providing ultrashort pulses in the short-, mid-, and long-wave infrared spectral regions as well as the deep UV [76–81]. Expanding the d-scan technique to different carrier wavelengths is a subject of ongoing research (see, e.g., [60] for the UV and [50] for the mid-infrared spectral ranges), and, without a doubt, we will see more work in this direction in the future.

REFERENCES

1. W. E. Lamb, "Theory of an optical maser," Phys. Rev. **134**, A1429–A1450 (1964).
2. E. P. Ippen, C. V. Shank, and A. Dienes, "Passive mode locking of the CW dye laser," Appl. Phys. Lett. **21**, 348–350 (1972).
3. P. F. Moulton, "Spectroscopic and laser characteristics of Ti:Al$_2$O$_3$," J. Opt. Soc. Am. B **3**, 125–133 (1986).

4. D. Strickland and G. Mourou, "Compression of amplified chirped optical pulses," Opt. Commun. **56**, 219–221 (1985).

5. D. E. Spence, P. N. Kean, and W. Sibbett, "60-fsec pulse generation from a self-mode-locked Ti:sapphire laser," Opt. Lett. **16**, 42–44 (1991).

6. R. L. Fork, C. H. B. Cruz, P. C. Becker, and C. V. Shank, "Compression of optical pulses to six femtoseconds by using cubic phase compensation," Opt. Lett. **12**, 483–485 (1987).

7. M. Nisoli, S. D. Silvestri, and O. Svelto, "Generation of high energy 10 fs pulses by a new pulse compression technique," Appl. Phys. Lett. **68**, 2793 (1996).

8. M. Nisoli, S. D. Silvestri, O. Svelto, R. Szipöcs, K. Ferencz, C. Spielmann, S. Sartania, and F. Krausz, "Compression of high-energy laser pulses below 5 fs," Opt. Lett. **22**, 522–524 (1997).

9. G. G. Paulus, F. Grasbon, H. Walther, P. Villoresi, M. Nisoli, S. Stagira, E. Priori, and S. De Silvestri, "Absolute-phase phenomena in photo-ionization with few-cycle laser pulses," Nature **414**, 182–184 (2001).

10. A. Schiffrin, T. Paasch-Colberg, N. Karpowicz, V. Apalkov, D. Gerster, S. Mühlbrandt, M. Korbman, J. Reichert, M. Schultze, S. Holzner, J. V. Barth, R. Kienberger, R. Ernstorfer, V. S. Yakovlev, M. I. Stockman, and F. Krausz, "Optical-field-induced current in dielectrics," Nature **493**, 70–74 (2013).

11. A. McPherson, G. Gibson, H. Jara, U. Johann, T. S. Luk, I. A. McIntyre, K. Boyer, and C. K. Rhodes, "Studies of multiphoton production of vacuum-ultraviolet radiation in the rare gases," J. Opt. Soc. Am. B **4**, 595–601 (1987).

12. M. Ferray, A. L'Huillier, X. Li, L. Lompre, G. Mainfray, and C. Manus, "Multiple-harmonic conversion of 1064 nm radiation in rare gases," J. Phys. B **21**, L31 (1988).

13. P. M. Paul, E. S. Toma, P. Breger, G. Mullot, F. Augé, Ph. Balcou, H. G. Muller, and P. Agostini, "Observation of a train of attosecond pulses from high harmonic generation," Science **292**, 1689–1692 (2001).

14. M. Hentschel, R. Kienberger, C. Spielmann, G. A. Reider, N. Milosevic, T. Brabec, P. Corkum, U. Heinzmann, M. Drescher, and F. Krausz, "Attosecond metrology," Nature **414**, 509–513 (2001).

15. T. Gaumnitz, A. Jain, Y. Pertot, M. Huppert, I. Jordan, F. Ardana-Lamas, and H. J. Wörner, "Streaking of 43-attosecond soft-x-ray pulses generated by a passively CEP-stable mid-infrared driver," Optics Express **25**, 27506–27518 (2017).

16. E. Goulielmakis, M. Uiberacker, R. Kienberger, A. Baltuska, V. Yakovlev, A. Scrinzi, T. Westerwalbesloh, U. Kleineberg, U. Heinzmann, M. Drescher, and F. Krausz, "Direct measurement of light waves," Science **305**, 1267–1269 (2004).

17. K. T. Kim, C. Zhang, A. D. Shiner, B. E. Schmidt, F. Légaré, D. M. Villeneuve, and P. B. Corkum, "Petahertz optical oscilloscope," Nat. Photonics **7**, 958–962 (2013).

18. S. B. Park, K. Kim, W. Cho, S. I. Hwang, I. Ivanov, C. H. Nam, and K. T. Kim, "Direct sampling of a light wave in air," Optica **5**, 402–408 (2018).

19. S. Keiber, S. Sederberg, A. Schwarz, M. Trubetskov, V. Pervak, F. Krausz, and N. Karpowicz, "Electro-optic sampling of near-infrared waveforms," Nat. Photonics **10**, 159–162 (2016).

20. E. P. Ippen and C. V. Shank, "Techniques for Measurement," in *Ultrashort Light Pulses: Picosecond Techniques and Applications* (Springer, 1977), pp. 83–122.

21. J.-H. Chung and A. M. Weiner, "Ambiguity of ultrashort pulse shapes retrieved from the intensity autocorrelation and the power spectrum," IEEE J. Sel. Top. Quantum Electron. **7**, 656–666 (2001).

22. D. J. Kane and R. Trebino, "Characterization of arbitrary femtosecond pulses using frequency-resolved optical gating," IEEE J. Quantum Electron. **29**, 571–579 (1993).

23. R. Trebino and D. J. Kane, "Using phase retrieval to measure the intensity and phase of ultrashort pulses: frequency-resolved optical gating," J. Opt. Soc. Am. A **10**, 1101–1111 (1993).

24. R. Trebino, *Frequency-Resolved Optical Gating: The Measurement of Ultrashort Laser Pulses* (Kluwer Academic, 2000).

25. C. Iaconis and I. A. Walmsley, "Spectral phase interferometry for direct electric field reconstruction of ultrashort optical pulses," Opt. Lett. **23**, 792–794 (1998).

26. A. S. Wyatt, I. A. Walmsley, G. Stibenz, and G. Steinmeyer, "Sub-10 fs pulse characterization using spatially encoded arrangement for spectral phase interferometry for direct electric field reconstruction," Opt. Lett. **31**, 1914–1916 (2006).

27. M. Anderson, A. Monmayrant, S.-P. Gorza, P. Wasylczyk, and I. Walmsley, "Spider: a decade of measuring ultrashort pulses," Laser Phys. Lett. **5**, 259–266 (2008).

28. V. V. Lozovoy, I. Pastirk, and M. Dantus, "Multiphoton intrapulse interference. IV. Ultrashort laserpulse spectral phase characterization and compensation," Opt. Lett. **29**, 775–777 (2004).

29. S. Grabielle, N. Forget, S. Coudreau, T. Oksenhendler, D. Kaplan, J.-F. Hergott, and O. Gobert, "Local spectral compression method for CPA lasers," in *CLEO/Europe and EQEC Conference Digest* (Optical Society of America, 2009), paper CF_P17.

30. V. Loriot, G. Gitzinger, and N. Forget, "Self-referenced characterization of femtosecond laser pulses by chirp scan," Opt. Express **21**, 24879–24893 (2013).

31. M. Miranda, T. Fordell, C. Arnold, A. L'Huillier, and H. Crespo, "Simultaneous compression and characterization of ultrashort laser pulses using chirped mirrors and glass wedges," Opt. Express **20**, 688–697 (2012).

32. M. Miranda, C. L. Arnold, T. Fordell, F. Silva, B. Alonso, R. Weigand, A. L'Huillier, and H. Crespo, "Characterization of broadband few-cycle laser pulses with the d-scan technique," Opt. Express **20**, 18732–18743 (2012).

33. D. E. Wilcox and J. P. Ogilvie, "Comparison of pulse compression methods using only a pulse shaper," J. Opt. Soc. Am. B **31**, 1544–1554 (2014).

34. C. S. Gonçalves, A. S. Silva, D. Navas, M. Miranda, F. Silva, H. Crespo, and D. S. Schmool, "A dual-colour architecture for pump-probe spectroscopy of ultrafast magnetization dynamics in the sub-10-femtosecond range," Sci. Rep. **6**, 22872 (2016).

35. C. Maibohm, F. Silva, E. Figueiras, P. T. Guerreiro, M. Brito, R. Romero, H. Crespo, and J. B. Nieder, "SyncRGB-FLIM: synchronous fluorescence imaging of red, green and blue dyes enabled by ultra-broadband few-cycle laser excitation and fluorescence lifetime detection," Biomed. Opt. Express **10**, 1891–1904 (2019).

36. D. Guénot, D. Gustas, A. Vernier, B. Beaurepaire, F. Böhle, M. Bocoum, M. Lozano, A. Jullien, R. Lopez-Martens, A. Lifschitz, and J. Faure, "Relativistic electron beams driven by kHz single-cycle light pulses," Nat. Photonics **11**, 293–296 (2017).

37. S. Mikaelsson, J. Vogelsang, C. Guo, I. Sytcevich, A.-L. Viotti, F. Langer, Y.-C. Cheng, S. Nandi, W. Jin, A. Olofsson, R. Weissenbilder, J. Mauritsson, A. L'Huillier, M. Gisselbrecht, and C. L. Arnold, "A high-repetition rate attosecond light source for time-resolved coincidence spectroscopy," Nanophotonics **10**, 117–128 (2021).

38. A. Weiner, "Effect of group velocity mismatch on the measurement of ultrashort optical pulses via second harmonic generation," IEEE J. Quantum Electron. **19**, 1276–1283 (1983).

39. A. Baltuska, M. S. Pshenichnikov, and D. A. Wiersma, "Second-harmonic generation frequency-resolved optical gating in the single-cycle regime," IEEE J. Quantum Electron. **35**, 459–478 (1999).

40. E. C. Jarque, J. S. Roman, F. Silva, R. Romero, W. Holgado, M. A. Gonzalez-Galicia, B. Alonso, I. J. Sola, and H. Crespo, "Universal route to optimal few- to single-cycle pulse generation in hollow-core fiber compressors," Sci. Rep. **8**, 2256 (2018).

41. F. Silva, B. Alonso, W. Holgado, R. Romero, J. S. Román, E. C. Jarque, H. Koop, V. Pervak, H. Crespo, and I. J. Sola, "Strategies for achieving intense single-cycle pulses with in-line post-compression setups," Opt. Lett. **43**, 337–340 (2018).

42. B. Alonso, I. Sola, and H. Crespo, "Self-calibrating d-scan: measuring ultrashort laser pulses on-target using an arbitrary pulse compressor," Sci. Rep. **8**, 3264 (2018).

43. B. Alonso, S. Torres-Peiró, R. Romero, P. T. Guerreiro, A. Almagro-Ruiz, H. Muñoz Marco, P. Pérez-Millán, and H. Crespo, "Detection and elimination of pulse train instabilities in broadband fibre lasers using dispersion scan," Sci. Rep. **10**, 7242 (2020).

44. E. Escoto, A. Tajalli, T. Nagy, and G. Steinmeyer, "Advanced phase retrieval for dispersion scan: a comparative study," J. Opt. Soc. Am. B **35**, 8–19 (2018).

45. A. Baltuska, A. Pugzlys, M. Pshenichnikov, and D. Wiersma, "Rapid amplitude-phase reconstruction of femtosecond pulses from intensity autocorrelation and spectrum," in *Technical Digest. Summaries*

of Papers Presented at the Conference on Lasers and Electro-Optics. Postconference Edition. CLEO '99. Conference on Lasers and Electro-Optics (1999), pp. 264–265.

46. R. W. Gerchberg and W. O. Saxton, "A practical algorithm for the determination of phase from image and diffraction plane pictures," Optik **35**, 237–246 (1972).

47. D. J. Kane, "Real-time measurement of ultrashort laser pulses using principal component generalized projections," IEEE J. Sel. Top. Quantum Electron. **4**, 278–284 (1998).

48. D. Kane, "Principal components generalized projections: a review," J. Opt. Soc. Am. B **25**, A120–A132 (2008).

49. N. C. Geib, M. Zilk, T. Pertsch, and F. Eilenberger, "Common pulse retrieval algorithm: a fast and universal method to retrieve ultrashort pulses," Optica **6**, 495–505 (2019).

50. N. C. Geib, R. Hollinger, E. Haddad, P. Herrmann, F. Légaré, T. Pertsch, C. Spielmann, M. Zürch, and F. Eilenberger, "Discrete dispersion scan setup for measuring few-cycle laser pulses in the mid-infrared," Opt. Lett. **45**, 5295–5298 (2020).

51. M. Miranda, J. Penedones, C. Guo, A. Harth, M. Louisy, L. Neoričić, A. L'Huillier, and C. L. Arnold, "Fast iterative retrieval algorithm for ultrashort pulse characterization using dispersion scans," J. Opt. Soc. Am. B **34**, 190–197 (2017).

52. T. Zahavy, A. Dikopoltsev, D. Moss, G. I. Haham, O. Cohen, S. Mannor, and M. Segev, "Deep learning reconstruction of ultrashort pulses," Optica **5**, 666–673 (2018).

53. S. Kleinert, A. Tajalli, T. Nagy, and U. Morgner, "Rapid phase retrieval of ultrashort pulses from dispersion scan traces using deep neural networks," Opt. Lett. **44**, 979–982 (2019).

54. O. Pérez-Benito and R. Weigand, "Nano-dispersion-scan: measurement of sub-7-fs laser pulses using second-harmonic nanoparticles," Opt. Lett. **44**, 4921–4924 (2019).

55. F. Silva, M. Miranda, B. Alonso, J. Rauschenberger, V. Pervak, and H. Crespo, "Simultaneous compression, characterization and phase stabilization of GW-level 1.4 cycle VIS-NIR femtosecond pulses using a single dispersion-scan setup," Opt. Express **22**, 10181–10191 (2014).

56. M. Miranda, F. Silva, L. Neoričić, C. Guo, V. Pervak, M. Canhota, A. S. Silva, I. J. Sola, R. Romero, P. T. Guerreiro, A. L'Huillier, C. L. Arnold, and H. Crespo, "All-optical measurement of the complete waveform of octave-spanning ultrashort light pulses," Opt. Lett. **44**, 191–194 (2019).

57. F. Silva, M. Miranda, S. Teichmann, M. Baudisch, M. Massicotte, F. Koppens, J. Biegert, and H. Crespo, "Pulse measurement from near to mid-IR using third harmonic generation dispersion scan in multilayer graphene," in *Conference on Lasers and Electro-Optics–International Quantum Electronics Conference* (Optical Society of America, 2013), paper CFIE_3_5.

58. M. Hoffmann, T. Nagy, T. Willemsen, M. Jupé, D. Ristau, and U. Morgner, "Pulse characterization by THG d-scan in absorbing nonlinear media," Opt. Express **22**, 5234–5240 (2014).

59. A. Tajalli, B. Chanteau, M. Kretschmar, H. Kurz, D. Zuber, M. Kovačev, U. Morgner, and T. Nagy, "Few-cycle optical pulse characterization via cross-polarized wave generation dispersion scan technique," Opt. Lett. **41**, 5246–5249 (2016).

60. A. Tajalli, T. K. Kalousdian, M. Kretschmar, S. Kleinert, U. Morgner, and T. Nagy, "Full characterization of 8 fs deep UV pulses via a dispersion scan," Opt. Lett. **44**, 2498–2501 (2019).

61. M. Canhota, F. Silva, R. Weigand, and H. M. Crespo, "Inline self-diffraction dispersion-scan of over octave-spanning pulses in the single-cycle regime," Opt. Lett. **42**, 3048–3051 (2017).

62. A.-L. Viotti, B. Hessmo, S. Mikaelsson, C. Guo, C. Arnold, A. L'Huillier, B. Momgaudis, A. Melninkaitis, F. Laurell, and V. Pasiskevicius, "Soliton self-compression and spectral broadening of 1 μm femtosecond pulses in single-domain KTiOPO₄," in *Conference on Lasers and Electro-Optics Europe and European Quantum Electronics Conference* (Optical Society of America, 2019), paper CF_4_5.

63. F. Böhle, M. Kretschmar, A. Jullien, M. Kovacs, M. Miranda, R. Romero, H. Crespo, U. Morgner, P. Simon, R. Lopez-Martens, and T. Nagy, "Compression of CEP-stable multi-mJ laser pulses down to 4fs in long hollow fibers," Laser Phys. Lett. **11**, 095401 (2014).

64. P. Rudawski, A. Harth, C. Guo, E. Lorek, M. Miranda, C. Heyl, E. Larsen, J. Ahrens, O. Prochnow, T. Binhammer, U. Morgner, J. Mauritsson, A. L'Huillier, and C. L. Arnold, "Carrier-envelope phase dependent high-order harmonic generation with a high-repetition rate OPCPA-system," Eur. Phys. J. D **69**, 70 (2015).

65. A. Harth, C. Guo, Y.-C. Cheng, A. Losquin, M. Miranda, S. Mikaelsson, C. M. Heyl, O. Prochnow, J. Ahrens, U. Morgner, A. L'Huillier, and C. L. Arnold, "Compact 200 kHz HHG source driven by a few-cycle OPCPA," J. Opt. **20**, 014007 (2017).

66. B. Alonso, W. Holgado, and I. J. Sola, "Compact in-line temporal measurement of laser pulses with amplitude swing," Opt. Express **28**, 15625–15640 (2020).

67. D. J. Kane and R. Trebino, "Single-shot measurement of the intensity and phase of an arbitrary ultrashort pulse by using frequency-resolved optical gating," Opt. Lett. **18**, 823–825 (1993).

68. D. Fabris, W. Holgado, F. Silva, T. Witting, J. W. G. Tisch, and H. Crespo, "Single-shot implementation of dispersion-scan for the characterization of ultrashort laser pulses," Opt. Express **23**, 32803–32808 (2015).

69. M. Louisy, C. Guo, L. Neoričić, S. Zhong, A. L'Huillier, C. L. Arnold, and M. Miranda, "Compact single-shot d-scan setup for the characterization of few-cycle laser pulses," Appl. Opt. **56**, 9084–9089 (2017).

70. A. Korobenko, P. Rosenberger, J. Schötz, A. Yu. Naumov, D. M. Villeneuve, M. F. Kling, A. Staudte, P. B. Corkum, and B. Bergues, "Single-shot dispersion sampling for optical pulse reconstruction," Opt. Express **29**, 11845–11853 (2021).

71. F. J. Salgado-Remacha, B. Alonso, H. Crespo, C. Cojocaru, J. Trull, R. Romero, M. López-Ripa, P. T. Guerreiro, F. Silva, M. Miranda, A. L'Huillier, C. L. Arnold, and I. J. Sola, "Single-shot d-scan technique for ultrashort laser pulse characterization using transverse second-harmonic generation in random nonlinear crystals," Opt. Lett. **45**, 3925–3928 (2020).

72. M. Czerny and A. F. Turner, "Über den astigmatismus bei spiegelspektrometern," Z. Phys. **61**, 792–797 (1930).

73. B. Bates, M. McDowell, and A. C. Newton, "Correction of astigmatism in a Czerny–Turner spectrograph using a plane grating in divergent illumination," J. Phys. E **3**, 206–210 (1970).

74. D. R. Austin, T. Witting, and I. A. Walmsley, "Broadband astigmatism-free Czerny–Turner imaging spectrometer using spherical mirrors," Appl. Opt. **48**, 3846–3853 (2009).

75. K.-S. Lee, K. P. Thompson, and J. P. Rolland, "Broadband astigmatism-corrected Czerny–Turner spectrometer," Opt. Express **18**, 23378–23384 (2010).

76. J. Li, X. Ren, Y. Yin, K. Zhao, A. Chew, Y. Cheng, E. Cunningham, Y. Wang, S. Hu, Y. Wu, M. Chini, and Z. Chang, "53-attosecond x-ray pulses reach the carbon K-edge," Nat. Commun. **8**, 186 (2017).

77. J. Pupeikis, P.-A. Chevreuil, N. Bigler, L. Gallmann, C. R. Phillips, and U. Keller, "Water window soft x-ray source enabled by a 25 W few-cycle 2.2 μm OPCPA at 100 kHz," Optica **7**, 168–171 (2020).

78. G. Andriukaitis, T. Balčiūnas, S. Ališauskas, A. Pugžlys, A. Baltuška, T. Popmintchev, M.-C. Chen, M. M. Murnane, and H. C. Kapteyn, "90 GW peak power few-cycle mid-infrared pulses from an optical parametric amplifier," Opt. Lett. **36**, 2755–2757 (2011).

79. M. Bock, L. von Grafenstein, U. Griebner, and T. Elsaesser, "Generation of millijoule few-cycle pulses at 5 μm by indirect spectral shaping of the idler in an optical parametric chirped pulse amplifier," J. Opt. Soc. Am. B **35**, C18–C24 (2018).

80. F. Reiter, U. Graf, M. Schultze, W. Schweinberger, H. Schröder, N. Karpowicz, A. M. Azzeer, R. Kienberger, F. Krausz, and E. Goulielmakis, "Generation of sub-3 fs pulses in the deep ultraviolet," Opt. Lett. **35**, 2248–2250 (2010).

81. M. Galli, V. Wanie, D. P. Lopes, E. P. Månsson, A. Trabattoni, L. Colaizzi, K. Saraswathula, A. Cartella, F. Frassetto, L. Poletto, F. Légaré, S. Stagira, M. Nisoli, R. Martínez Vázquez, R. Osellame, and F. Calegari, "Generation of deep ultraviolet sub-2-fs pulses," Opt. Lett. **44**, 1308–1311 (2019).